Solution Structure of the Lyase Domain of Human DNA Polymerase λ

Eugene F. DeRose,‡ Thomas W. Kirby,‡ Geoffrey A. Mueller,‡ Katarzyna Bebenek,‡ Miguel Garcia-Diaz,§ Luis Blanco,§ Thomas A. Kunkel,‡ and Robert E. London*,‡

Laboratory of Structural Biology, National Institute of Environmental Health Sciences, National Institutes of Health, Box 12233, Research Triangle Park, North Carolina 27709, and Centro de Biologia Molecular Severo Ochoa (CSIC-UAM), Universidad Autonoma, 28049 Madrid, Spain

Received February 21, 2003; Revised Manuscript Received June 13, 2003

ABSTRACT: DNA polymerase λ (pol λ) is a recently discovered nuclear enzyme belonging to the pol X family of DNA polymerases that exhibits a 32% sequence identity with the nuclear DNA repair protein, pol β. Structural modeling suggests that pol λ contains the palm, fingers, thumb, and 8 kDa lyase domains present in pol β, as well as an additional N-terminal BRCT domain and a serine−proline-rich linker that are presumably involved in protein−protein interactions. The 8 kDa domain of pol β is important for DNA binding and contains the dRP lyase activity, which is the rate-limiting step in the single-nucleotide base excision repair (BER) pathway of damaged DNA. Recently, it was shown that the 8 kDa domain of pol λ also contains the dRP lyase activity. To gain further insight into the catalytic mechanism of dRP removal by pol λ, we have determined the solution structure of the 8 kDa lyase domain of human DNA pol λ via multidimensional NMR methods and the ARIA program. The resulting structures exhibited a high degree of similarity with the 8 kDa lyase domain of pol β. Specifically, the side chains of residues W274, R275, Y279, K307, R308, and K312 are in similar positions to the functionally important side chains of residues H34, K35, Y39, K60, K68, and K72 in the 8 kDa lyase domain of pol β. This suggests that, on the basis of the proposed roles of these residues in pol β, the corresponding pol λ side chains may be involved in DNA binding and dRP lyase activity. The structural alignment of W274 (pol λ) with H34 (pol β) indicates that the former is probably involved in a similar base stacking interaction with template DNA at the position of the gap, in contrast with several previous proposals which aligned D272 with H34. In a few cases for which there is a nonconservative substitution in the sequence alignment, a structural comparison shows a positionally and, hence, probably a functionally equivalent residue, e.g., K60 in pol β and K307 in pol λ. Additionally, on the basis of the structural alignment obtained, several previously proposed mechanistic hypotheses can be evaluated.

An understanding of the enzymatic basis of DNA repair is of critical importance for the development of insights into how physical and chemical agents alter cellular DNA. DNA polymerase λ (pol λ) is a recently identified nuclear enzyme that is present in mammals as well as other vertebrates and plants (*1*−*5*). It shares a 32% amino acid identity with pol β, and structural modeling suggests that pol λ contains the palm, fingers, thumb, and 8kDa domains present in pol β. The primary distinction of pol λ is the presence of an additional N-terminal BRCT domain, which presumably is involved in protein−protein or protein−DNA interactions, and a serine−proline-rich linker region (*2*, *5*). The BRCT domain of pol λ is predicted to include residues 35−125, while the sequence homologous with pol β includes residues 241−575. Pol λ has DNA polymerase (*2*) and dRP lyase (*4*) activities and synthesizes DNA distributively on an open template-primer DNA and processively on substrates containing short gaps (*5*). The level of processivity is enhanced in gapped DNA containing a 5′-phosphate on the downstream strand (*5*). Thus its catalytic and DNA binding properties are similar to those of pol β.

The 8 kDa lyase domain of pol β, consisting of the N-terminal 87 residues of the enzyme, was originally identified as a spontaneous proteolytic product (*6*). It is responsible for most of the DNA binding activity of pol β. This domain has been of considerable recent interest since it not only supplies an important structural element for the polymerization reaction, being essential for correct positioning of the enzyme in gapped substrates (*7*, *8*), but also contains the important dRP lyase catalytic activity of the enzyme (*9*−*13*). The dRP lyase reaction is of critical importance, because it is the rate-determining step in single-nucleotide BER of apurinic/apyrmidinic (AP) sites in damaged DNA by pol β (*14*). In addition, it has been found that the dRP lyase activity of pol β is required to reverse methylating agent hypersensitivity in fibroblasts from pol β null mice (*15*), indicating that removal of the dRP moiety, by the lyase domain, is a crucial step in BER of DNA alkylation damage *in vivo*.

Three sequence alignments of pol λ with pol β have been proposed that are generally similar but differ in a few specific regions, as shown in Figure 1. In particular, H34 in pol β aligns with W274 of pol λ, according to the alignment given

* To whom correspondence should be addressed. Phone: 919-541-4879. Fax: 919-541-5707. E-mail: london@niehs.nih.gov.
‡ National Institutes of Health.
§ Universidad Autonoma.

10.1021/bi034298s CCC: $25.00
Published on Web 07/25/2003

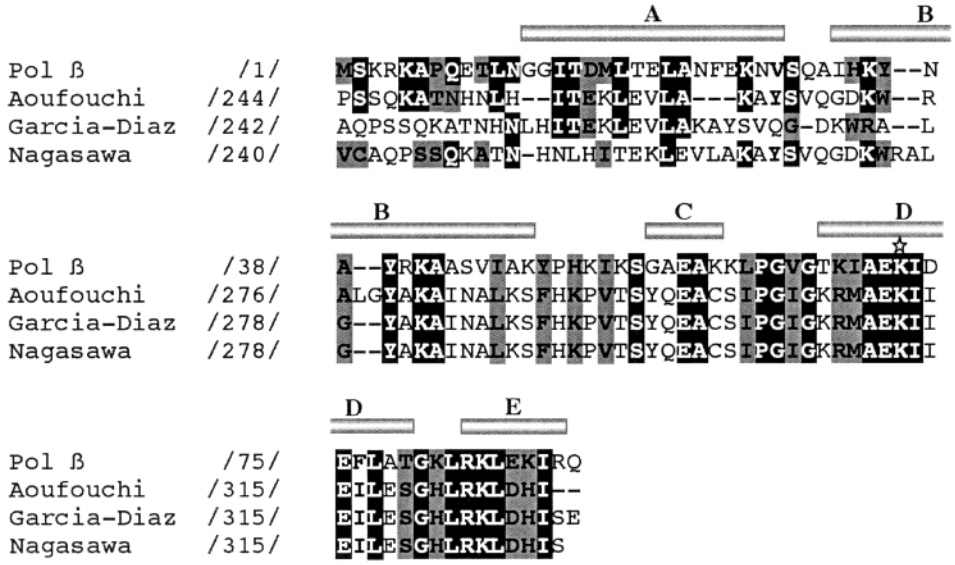

FIGURE 1: Alignment of the 8 kDa domains of pol β and pol λ. The first row shows the sequence of human pol β, and the last three rows show the alignment of human pol λ proposed by Aoufouchi (*1*), Garcia-Diaz (*4*, *5*), and Nagasawa (*3*). The helix positions indicated by the bars above the pol β sequence correspond to the crystal structure of pol β (*17*) and are labeled A, B, C, etc., following the convention used in the pol β literature. Helix E (residues 83−89 in pol β) is present in the X-ray structure of the complete pol β protein but is not observed in the solution structure of the 8 kDa domain (*18*, *19*), because the domain is terminated at K87 in the middle of helix E, corresponding to the spontaneous proteolytic product (*6*). K87 corresponds to H327 in pol λ. Pol λ residues that are aligned with identical residues in pol β are indicated by white letters on a black background. Conservative alignments of pol λ residues with pol β are indicated by bold letters on a gray background, with conservative residues grouped as follows: GASTCP; RKH; DE; MVIL; FYWH.

by Garcia-Diaz et al. (*2*, *4*, *5*), and with D272 of pol λ, following the alignments of Aoufouchi et al. (*1*) and Nagasawa et al. (*3*). A resolution of this discrepancy in alignments is important, because H34 is involved in a critical base stacking interaction with the downstream template base of gapped DNA that facilitates bending of the DNA axis by 90° (*8*; 1BPX). A structural alignment (*2*) using the Swiss Model software (*16*) and the known pol β crystal structure (*17*) identified only three of the four helices present in the solution structure (*18*, *19*) of the lyase domain of pol β. The fifth helix in the crystal structure of pol β (helix E in Figure 1) is absent in solution, presumably due to termination of the domain at K87 in the middle of this helix. In addition to the questions that the alignments raise regarding the interaction with DNA, it is important to determine whether other residues thought to play a catalytic role in the dRP lyase activity and DNA binding align in the pol β and pol λ structures. Thus, to gain further understanding of the catalytic mechanism of dRP removal, we have determined the solution structure of the 8 kDa lyase domain of human pol λ using multidimensional NMR methods.

EXPERIMENTAL PROCEDURES

Cloning and Expression. A 265-nucleotide *Nde*I−*Hin*dIII restriction fragment was ligated into pET30a(+) (Novagen) to allow for the expression of an 87 amino acid peptide corresponding to residues 242−327 of human DNA pol λ. The construct, dubbed pET30lambda8K, selected on the basis of its alignment with residues 1−87 of the 8 kDa domain of pol β (*4*), was transformed into *Escherichia coli* strain BLR-(DE3). Cells containing the plasmid were grown to mid-log phase (A_{600} = ~0.6) at 37 °C in M9 minimal medium containing 50 μg/mL kanamycin, ^{15}N-labeled ammonium chloride, and either ^{13}C-labeled glucose or unlabeled glucose. Peptide expression was induced by addition of isopropyl thio-β-D-galactoside (IPTG) to 1 mM, and the growth was continued for 3 h. The cells were harvested by centrifugation and stored at −20 °C.

Purification. The frozen cell pellet was thawed and resuspended in 50 mM Tris, pH 7.5, 1 mM EDTA, 1 mM DTT, and 500 mM NaCl, and cells were lysed by sonication in a Branson sonifier 200 using a microtip probe at output level of 6 for 10 × 30 s with 30 s cooling. The lysate was centrifuged at 30000*g* for 15 min, and then nucleic acid precipitation was effected by addition of solid streptomycin sulfate to a final concentration of 10 mg/mL. After 30 min on ice the suspension was again centrifuged at 30000*g* for 15 min. The supernatant was diluted with buffer (50 mM Tris, pH 7.5, 1 mM EDTA, 1 mM DTT) to give a final concentration of 75 mM NaCl, and the mixture was pumped onto a column (2.6 × 35 cm) containing Q-Sepharose (Amersham), which was connected to another column (1.6 × 13 cm) containing single-stranded DNA−cellulose (Sigma). The columns were washed with 1 column volume of buffer (50 mM Tris, pH 7.5, 1 mM EDTA, 1 mM DTT, 75 mM NaCl), and then the DNA−cellulose column was disconnected from the Q-Sepharose column, and the latter was eluted with a gradient of 75−1000 mM NaCl. Fractions containing the 8 kDa domain of pol λ were identified by SDS−polyacrylamide gel electrophoresis, pooled, and concentrated to a volume of 5 mL using a Centricon YM-3 filter unit (Millipore). The protein was chromatographed on a 2.6 × 63 cm column of Sephacryl S-100, which was eluted with 50 mM Tris, pH 7.5, 1 mM EDTA, 1 mM DTT, and 75 mM NaCl. Fractions containing the 8 kDa domain were pooled and loaded onto an FPLC column (2.6 × 15 cm) containing SP-Sepharose (Amersham) and eluted with a gradient of 75−1000 mM NaCl. The pure pol λ 8 kDa domain protein was concentrated, and NMR samples were

prepared. The samples typically contained 2 mM protein in 5 mM Tris-d_{11}, pH 7, 100 mM NaCl, 1 mM deuterated DTT, 5 mM NaN_3, 10% D_2O, and 0.5 μL of Calbiochem protease inhibitor cocktail set III per 600 μL sample.

NMR Studies. The NMR experiments were performed on a Varian 600 MHz UNITY*INOVA* spectrometer, using a 5 mm Varian $^1H\{^{13}C,^{15}N\}$ triple resonance probe with actively shielded *z*-axis gradients and variable temperature capability. All NMR experiments were conducted at 25 °C. The NMR data were processed using NMRPipe (*20*) and spectra analyzed using NMRView (*21*). The sequential backbone and Cβ resonance assignments were made from a combined analysis of HNCACB (*22*, *23*), CBCA(CO)NH (*23*, *24*), and HNCO (*25*, *26*) experiments. The HNCACB, CBCA(CO)-NH, and HNCO spectra were acquired using Varian's ghn_cacb, gcbca_co_nh, and ghn_co ProteinPack sequences. Side-chain proton and carbon chemical shift assignments were made from an analysis of H(CCO)NH-TOCSY and (H)C(CO)NH-TOCSY spectra (*27*−*30*), acquired using the pulse sequences described by Gardner et al. (*31*), obtained from Lewis Kay. Phenylalanine and tyrosine Hδ, Cδ, Hϵ, amd Cϵ and tryptophan Hδ1 and Cδ1 resonances were assigned from a combined analysis of (HB)CB(CGCD)-HD, (HB)CB(CGCDCE)HE (*32*), and $^1H-^{13}C$ HSQC experiments. All 3D triple resonance experiments, including the TOCSY experiments, were processed using squared cosine bell apodization functions in all dimensions, and forward−backward (*33*) and mirror image linear prediction (*34*) in the indirect carbon and nitrogen dimensions, respectively, to double the number of points before Fourier transformation. A low-pass filter was used to suppress the solvent signal in all cases. Additional experimental details are provided as Supporting Information.

NOEs were assigned from 3D ^{15}N- and ^{13}C-edited NOESY spectra obtained using an improved version of the CN NOESY-HSQC experiment (*35*), obtained from Lewis Kay's group, in which the ^{15}N-edited NOESY spectrum is acquired with full resolution in the ^{15}N dimension. The CN NOESY-HSQC experiment was acquired with 128 × 36 × 512 complex points, with acquisition times of 16.0 ms, 10.0 and 20.0 ms, and 64.0 ms in t_1 (^1H), t_2 (^{13}C and ^{15}N), and t_3 (^1H), respectively, 16 scans per increment, using a 1 s delay between scans, with a 100.0 ms mixing time, resulting in a total acquisition time of approximately 180 h. In this experiment, the ^{13}C transmitter frequency is set to 67.0 ppm to pick up NOEs to the aromatic protons as well as the aliphatic protons. The spectra were processed with squared cosine bell apodization functions in all dimensions and forward−backward linear prediction (*33*) in the ^{15}N and ^{13}C dimensions.

Structure Calculations. The ARIA (*36*−*39*), version 1.1, and CNS (*40*), version 1.0, programs were used to compute the solution structure starting from an extended structure with random side-chain conformations. All NOE cross-peaks from the CN-NOESY-HSQC spectra and chemical shift assignments were used as input to ARIA. The NOE data sets were split into 3D H−CH and 3D H−NH data, and as many artifact peaks as possible were deleted manually. By default, ARIA calibrates distance restraints by computing the relaxation matrix from the NOE peak intensities and the chemical shift assignments (*41*). A rotational correlation time of 7.18 ns, computed for the 8 kDa domain of pol β (*19*), was used for computation of the relaxation matrix. More precise structures (i.e., structures with a lower mean RMSD) were obtained using the standard r^{-6} dependence of the NOE volumes and the isolated spin pair approximation implementation in ARIA to calibrate the distance restraints (*42*). ARIA uses ambiguous as well as unambiguous distance restraints. The total number of ambiguous NOE restraints allowed for each peak in the NOESY spectra was set to 20. Nine cycles of NOE generation by ARIA, followed by simulated annealing, were carried out. Simulated annealing used the standard CNS protocol (*40*, *41*), incorporating both torsion angle and Cartesian dynamics. Iteration zero is used to generate the initial ensemble of structures, with the NOE violation tolerance set to 1000 Å, to ensure that no NOE distance restraints are excluded, and with the partial assignment cutoff probability set to 1.01, to ensure that partial NOE assignments are based on chemical shifts only. In the next eight iterations the NOE violation tolerances are set to 1000.0, 1.0, 0.5, 0.1, 1.0, 0.1, 0.1, and 0.1 Å, and the partial assignment cutoff probabilities are set to 0.9999, 0.999, 0.99, 0.98, 0.96, 0.93, 0.90, and 0.80. Thus the NOE violation tolerance is reduced as the structure improves, with the exception of iteration 5, in which the tolerance is increased to 1.0 Å to ensure that important NOEs, consistent with the present structure, are not excluded. The partial assignment probability is also reduced in successive iterations to eliminate ambiguous NOEs, which make the smallest contribution to the current structure. These default ARIA parameters are similar to those given in Table 1 [Run1, Linge et al. (*41*)]. In the final iteration, ARIA assigned 790 unambiguous distance restraints and 191 ambiguous distance restraints. Of these, 244 were unique long-range and 36 ambiguous long-range distance restraints. ARIA did not converge to a unique structure, without the addition of supplemental manually assigned distance restraints. A total of 281 manually assigned NOE distance restraints (54 long range) were included in the calculation. Distance restraints, derived from the manually assigned NOEs, were set to 1.8−6.0 Å. In addition to the NOE restraints, 58 hydrogen bond restraints, based on CSI and TALOS (*43*) predictions of the locations of the α-helices, were included in the calculation. A total of 53 ϕ and ψ dihedral angle restraints were also used. The dihedral angle restraints were taken to be ±2 standard deviations or at least ±20° from the average values predicted by TALOS. CSI predictions were used to generate dihedral angle restraints for residues that did not meet TALOS acceptance criteria. In these cases, the dihedral angles were restrained to $\phi = -70°$ (±50°) and $\psi = -50°$ (±50°) for the α-helical regions. The average energy-minimized structure, as well as the ensemble of the seven lowest energy structures, was deposited in the Protein Data Bank, ID code 1NZP.

Initial $^1H-^{15}N$ HSQC spectra of the 8 kDa domain of pol λ, comprising residues 242−327, exhibited additional peaks, apparently due to hydrolysis of the C-terminal end of the protein. Three-dimensional NMR studies were therefore commenced using a protease inhibitor cocktail added directly to the sample. In addition, DTT was added to the samples, and the NMR tubes were sealed under argon gas to minimize oxidation of the sample. The 8 kDa domain contains one cysteine at position 300 and one methionine at position 309. Under these conditions, the protein was stable for several

Table 1: Statistics for the Structure Ensembles

ARIA NOEs	
H−CH	934
H−NH	403
unambiguous	790
ambiguous	191
total[a]	981
manual NOEs	
H−CH	229
H−NH	52
H-bonds	58
ensemble RMSD (Å)	
secondary structure (backbone)[b]	0.84 ± 0.35
secondary structure (heavy)[b]	1.67 ± 0.71
backbone (residues 254−320)[c]	0.93 ± 0.13
heavy atoms (residues 254−320)[c]	1.48 ± 0.15
average violations per structure	
NOEs and/or H-bonds	0.14 ± 0.38[d]
dihedrals	0
RMSD (experimental restraints)[b]	
NOEs (Å)	0.0233 ± 0.0046
H-bonds (Å)	0.0166 ± 0.0290
dihedral angles (deg)	0.11 ± 0.06
RMSD (covalent geometry)[b]	
bonds (Å)	0.0016 ± 0.0002
angles (deg)	0.2960 ± 0.0168
impropers (deg)	0.1534 ± 0.0150
Ramachandran space (%)[e]	
most favored region	80.7
additionally allowed	17.1
generously allowed	1.3
disallowed	0.9

[a] Total refers to the sum of the unambiguous and ambiguous restraints, which is not the same as the total NOEs assigned for each NOESY experiment. Ambiguous restraints can have multiple assignments, and redundant assignments from each experiment are filtered in this reported total. [b] Output by ARIA (*42*), calculated by CNS (*40*) using the ensemble of the seven lowest energy structures. [c] Average backbone RMSD of all structures with respect to the mean calculated with MOLMOL (*44*). [d] One NOE violation for the ensemble of seven lowest energy structures. [e] Calculated with PROCHECK (*50*, *51*). The percentages are computed over all seven lowest energy structures.

weeks at 25 °C. All of the NMR experiments were carried out on a 2 mM U-^{13}C,^{15}N-labeled sample.

RESULTS

The protein was almost completely assigned except for the N-terminal resonances 242−248. As observed with the pol β lyase domain (*18*, *19*), it is probable that the N-terminal region is disordered and may be undergoing comformational averaging, which may account for the presumed broadening of these unobserved resonances. The amide resonances of N251 and H290 also were not assigned. Since the amide resonances of A249 and T250 were very weak, suggestive of conformational exchange broadening, it is not surprising that the amide resonance of N251 was not observed. Although the amide resonances of N251 and H290 were not assigned, the Cα, Hα, and side-chain resonances of these residues were assigned from the CBCA(CO)NH, H(CCO)-NH-TOCSY, and (H)C(CO)NH-TOCSY spectra. Chemical shifts of all assigned resonances have been deposited in the BioMagResBank (http://www.bmrb.wisc.edu) under BMRB accession number BMRB-5766.

A CSI analysis of the Hα, Cα, Cβ, and C′ chemical shifts revealed four stretches of α-helical regions, extending from residues 254−269, 273−287, 296−300, and 307−320. Sequence positions for the pol λ and pol β 8 kDa lyase domains can be computed on the basis of the alignment of Garcia-Diaz et al. (*4*, *5*), Figure 1, by subtracting 241 from sequence positions 242−271 and subtracting 240 from sequence positions 272−327 of pol λ. Thus, the CSI helical regions correspond to residues 13−28, 33−47, 56−60, and 67−80 in the pol β sequence. The CSI secondary structure predictions are supported by a TALOS analysis of the sequence and chemical shifts, which predicts four continuous α-helical regions from 255−268, 273−286, 296−299, and 307−317, corresponding to residues 15−28, 33−46, 56−59, and 67−77 in the pol β sequence. These predictions agree well with the helical regions of the solution structure of the 8 kDa lyase domain of pol β (*19*), i.e., 15−28, 35−47, 56−61, and 68−78, as computed using MOLMOL (*44*), lending further support to the hypothesis that the two structures are similar.

There is some discrepancy in the CSI and TALOS predictions of the length of the fourth helix in pol λ, i.e., 307−320 (CSI) and 307−317 (TALOS). Part of this discrepancy arises because the amide resonance of H321 is very weak, and consequently, it was not possible to assign the C′ and Hα chemical shifts of G320, yet the CSI consensus considers G320 to be α-helical. In addition, TALOS found eight matches of the triplets including residues E318 and S319 in its database with α-helical conformation. However, since only predictions with at most one outlier were considered unambiguous, the backbone dihedral angles predicted by TALOS were not used in the calculation of the structure, *vide supra*. In addition, although strong sequential amide−amide NOEs were observed for residues L317, E318, and S319, no other NOEs indicative of α-helical secondary structure were observed for these resonances.

Twenty solution structures were generated using the combined ARIA/CNS protocol described above. The structural statistics for the seven lowest energy structures, generated by ARIA in the final iteration, are shown in Table 1. ARIA was able to assign 981 NOEs as categorized in Table 1. As described above, an additional 281 manually assigned NOEs were added to the calculation. Manual spot checks of the NOEs assigned by ARIA were performed to assess the accuracy of the assignments and were found to be consistent with the structure. In cases of extreme overlap ARIA often did not assign any NOEs. In particular, many methyl−methyl and methyl−aromatic NOEs between hydrophobic residues required manual assignment. The ensemble of the seven lowest energy structures exhibits a backbone pairwise RMSD of 0.84 ± 0.35 Å, for the α-helical regions, and mean backbone and heavy atom RMSDs of 0.93 ± 0.13 Å and 1.48 ± 0.15Å, respectively, for residues 254−320 (Table 1). The ensemble of seven lowest energy structures for residues 254−320 (RMSD 0.93 Å) are shown in Figure 2a. The four α-helical regions are shown in red, and a ribbon rendering of the average energy-minimized structure is shown in Figure 2b. In the average energy-minimized structure, the four α-helical regions comprise residues 255−270, 273−286, 296−300, and 307−317, which agrees well with the TALOS predictions, i.e., 255−268, 273−286, 296−299, and 307−317. The Ω loop connecting helices A and B is also indicated (*18*).

The solution structure of pol λ is similar to the crystal structure of the 8 kDa domain of pol β in the complete protein (PDB ID code 1BPD) (*17*). This is not surprising,

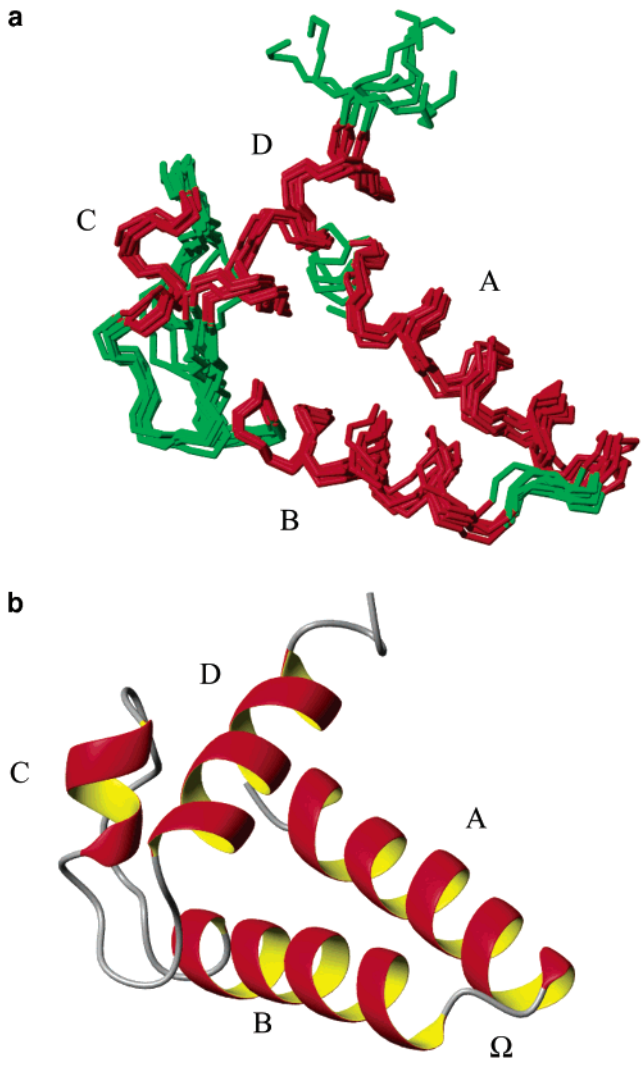

FIGURE 2: (a) Backbone overlay (residues 254−320) of the seven lowest energy structures of the pol λ 8 kDa domain exhibiting an average RMSD with respect to the mean structure of 0.93 ± 0.13 Å. The four helices are shown in red. (b) Ribbon rendering of the structure of the pol λ 8 kDa domain. All figures of the 8 kDa domains of pol λ and pol β were generated with MOLMOL (*44*).

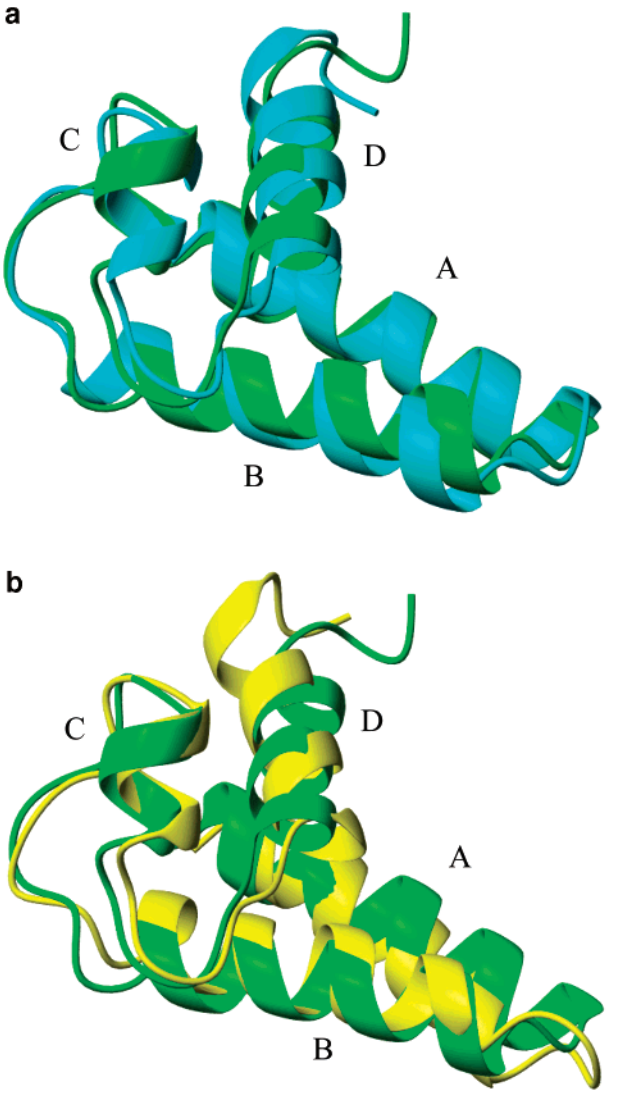

FIGURE 3: (a) Backbone superposition (residues 254−271 and 272−320) of the solution structure of the 8 kDa domains of pol λ (green) with the crystal structure [1BPD (*17*)] (residues 13−30 and 32−80) of pol β (cyan), demonstrating similarities and differences in the two structures. The structures superimposed with an RMSD of 1.46 Å. (b) Backbone superposition (residues 254−271 and 272−320) of the solution structure of the 8 kDa domains of pol λ (green) with the solution structure [1DK3 (*19*)] (residues 13−30 and 32−80) of the 8 kDa domain of pol β (yellow), demonstrating similarities and differences in the two structures. The structures superimposed with an RMSD of 2.04 Å. Both structures consist of two sets of antiparallel helices, with a loop region between helix A and helix B and a hairpin turn between helix C and helix D. Differences in the orientations of the helices between the pol λ structure and the two pol β structures are described in the text and further quantified in Table 2.

because the 8 kDa domain does not interact with rest of the protein in the X-ray structure of the complete protein (*17*). The 8 kDa domain interacts with the fingers subdomain of pol β upon binding gapped DNA and additionally with the thumb subdomain upon formation of the ternary complex with dNTP (*8*). Residues 254−271 and 272−320 of the average energy-minimized structure of the pol λ structure superimpose on residues 13−30 and 32−80 of the crystal structure of pol β, with a backbone RMSD of 1.46 Å. This superposition, shown in Figure 3a, is based on the sequential alignment given by Garcia-Diaz et al. (*4*, *5*). Both structures are comprised of two sets of antiparallel α-helices, i.e., A−B and C−D. [The helix labeling convention is taken from Sawaya et al. (*17*).] Helices A−B are connected by an Ω loop, and helices C−D are connected by a hairpin, forming a HhH DNA binding motif (*45*, *46*). [Elements of secondary structure also were identified using the program MOLMOL (*44*).] The HhH DNA binding motif of the 8 kDa lyase domain of pol β interacts with the downstream oligo in the crystal structure of pol β and gapped DNA (*8*). The hairpin interacts with the backbone of the oligo. The helical regions of the 8 kDa lyase domain of pol λ comprise residues 255−270 (A), 273−286 (B), 296−300 (C), and 307−317 (D), corresponding to sequence positions 14−29, 33−46, 56−60, and 67−77 in the pol β lyase domain. This agrees well with the α-helical regions of the crystal structure of the pol β lyase domain, i.e., 15−29 (A), 33−48 (B), 56−61 (C), and 67−78 (D). The position of the Ω loop connecting helices A and B, the long loop connecting helices B and C, and the hairpin turn connecting helices C and D forming an HhH DNA binding motif overlay remarkably well between the two structures (Figure 3a). Although the structures are very similar, there are some differences in the orientation of

Table 2: Comparison of Helix Crossing Angles

	crossing angle				
	pol β helix[a]	pol β helix[b]	pol λ helix	Δ (λ−β) helix[c]	Δ (λ−β) helix[d]
A−B	165.8	152.6	162.6	−3.2	10.0
A−C	68.5	51.7	71.0	2.5	19.3
A−D	122.0	147.8	113.3	−9.0	−34.5
B−C	102.0	103.0	91.9	−10.1	−11.1
B−D	62.9	50.6	75.4	12.5	24.8
C−D	155.9	149.6	131.7	−24.2	−17.9

[a] Lyase domain from crystal structure (1BPD). [b] Lyase domain from solution structure (1DK3). [c] Pol λ helix crossing angle minus pol β crystal structure helix crossing angle. [d] Pol λ helix crossing angle minus pol β solution structure helix crossing angle.

the α-helices. Table 2 contains the helix crossing angles for each of the two domains, as well as the change in helix crossing angles in the pol λ lyase domain, relative to the pol β lyase domain. From this table and Figure 3a, it is apparent that helix D in the solution structure of pol λ exhibits the greatest change in position, compared to the position of helix D in the X-ray structure of pol β. Thus, the crossing angle between helices B and D increases from 62.9° in the crystal structure of pol β to 75.4° in the solution structure of pol λ, a change of 12.5°. The crossing angle between helices C and D decreases from 155.9°, in the crystal structure of pol β, to 131.7°, in the solution structure of pol λ, a change of −24.2°. The remaining crossing angles are similar in the two structures.

The general agreement of the solution structure of the 8 kDa lyase domain of pol λ with the previously determined solution structure of this domain in pol β (*19*) is also very strong, although not quite as good as the agreement with the crystal structure of the latter (*17*) (Figure 3). In particular, residues 254−271 and 272−320 of the average energy-minimized structure of the pol λ structure superimpose on residues 13−30 and 32−80 of the solution structure of the 8 kDa domain of pol β (PDB ID code 1DK3) (*19*), with a backbone RMSD of 2.04 Å (Figure 3b). This backbone RMSD for the superposition of the two solution structures is slightly greater than the 1.46 Å RMSD for the superposition with the crystal structure (Figure 3a). The reasons for the better superposition with the X-ray structure are unclear, but the backbone RMSD between the X-ray structure of the 8 kDa domain of pol β in the complete protein (1BPD) and the solution structure of the isolated domain (1DK3) is 1.84 Å. Since the 8 kDa domain of pol β does not interact with the polymerase domain in the crystal structure (*17*), these differences cannot be attributed to this interaction. The position of the long loop connecting helices B and C and the hairpin turn connecting helices C and D of the HhH DNA binding motif overlay remarkably well between the two structures; however, there is some change in the position of the Ω loop in the structure of the pol λ domain, relative to its position in the pol β lyase domain. A comparison of panels a and b of Figure 3 and Table 2 shows that there is greater disparity in the position of the α-helices between the two solution structures than there is between the crystal structure of pol β and the solution structure of the pol λ domain. Thus, the crossing angle between helices A and D decreases from 147.8° in the solution structure of pol β to 113.3° in the solution structure of pol λ, a change of −34.5°. In comparison, the crossing angle changes by only −9.0° relative to the crystal structure of pol β. The crossing angle between helices B and D increases from 50.6°, in the solution structure of the pol β domain, to 75.4°, in the solution structure of the pol λ domain, a change of 24.8°, compared to a change of only 12.5° relative to the crystal structure of pol β. In general, the solution structure of the 8 kDa lyase domain of pol λ exhibits a slightly greater degree of similarity to the crystal structure of the pol β domain than to the solution structure of the pol β domain (Figure 3 and Table 2), though the differences are small.

DISCUSSION

DNA polymerase λ (pol λ) is a recently identified nuclear enzyme that is present in mammals as well as other vertebrates and plants (*1*−*3*). It shares a 32% amino acid identity with pol β, and structural modeling suggests that pol λ contains the palm, fingers, thumb, and 8 kDa domains present in pol β, as well as an additional domain that has no analogue in pol β (*2*, *5*). The 8 kDa domain has been of particular interest since the realization that this domain of pol β contains the dRP lyase activity of the enzyme. This reaction is the rate-limiting step in the repair of alkylation−DNA damage during base excision repair (*15*). The corresponding domain of pol λ has recently been shown to possess this activity (*4*). Hence, a structural comparison of the two domains can shed light on the involvement of the various residues in DNA binding and catalysis.

Structural Alignment of Pol λ with Pol β. Three groups have proposed alignments of human pol λ with pol β (*1*, *3*−*5*), and the relevant proposals for the 8 kDa domains are summarized in Figure 1. The alignments are identical for pol β amino acid residues Y39−I88 but differ for the preceding residues, including the important DNA binding and catalytic residues H34 and K35. In the alignment of Garcia-Diaz et al. (*5*), W274 and R275 of pol λ correspond to H34 and K35 of pol β, respectively. Nagasawa et al. (*3*) and Aoufouchi et al. (*1*) align D272, K273, and W274 of pol λ with H34, K35, and Y36 of pol β, respectively. Figure 4 shows the superposition of residues 254−320 of the average energy-minimized structure of pol λ and residues 13−80 of the crystal structure of pol β, aligned by calculating the superposition of residues 254−271 and 272−320 of pol λ with residues 13−30 and 32−80 of pol β. Also shown are the side chains of amino acid residues H34, K35, and Y36 of pol β, as well as the side chains of amino acid residues D272, K273, W274, and R275 of pol λ. It is clear from this "structural alignment" that the sequential alignment of Garcia-Diaz et al. (*4*, *5*) is correct. Residues W274 and R275 in the solution structure of the 8 kDa domain of pol λ occupy positions that are close to those of residues H34 and K35 in the crystal structure of pol β. The agreement between the positions of the other residues in the structured region of the two domains (i.e., residues 254−320 of pol λ and residues 14−80 of pol β) is also very good. In the crystal structure of pol β with gapped DNA [1BPX (*8*)], the imidazole ring of H34 forms a base stacking interaction with the exposed template base of the downstream side of the gap, which helps to stabilize the complex, and K35 is required for 5′-phosphate recognition in binding to gapped DNA (*11*). Therefore, analogous interactions with residues

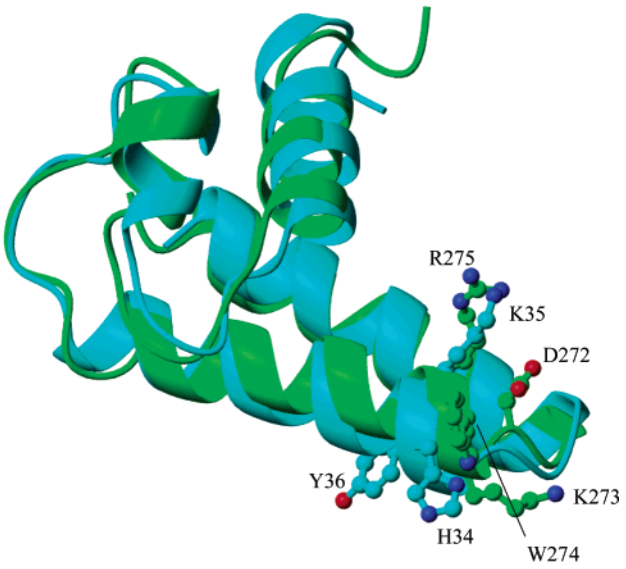

FIGURE 4: Ribbon diagrams illustrating the backbone superposition of the solution structure of the 8 kDa domains of pol λ (residues 254−271 and 272−320) (green) with the crystal structure of pol β [1BPD (*17*)] (residues 13−30 and 32−80) (cyan). Also shown are the side chains of amino acid residues H34, K35, and Y36 of pol β, as well as the side chains of amino acid residues D272, K273, W274, and R275 of pol λ. Residues W274 and R275 in the solution structure of the 8 kDa domain of pol λ are in very similar positions to residues H34 and K35 in the crystal structure of pol β, in agreement with the sequential alignment of Garcia-Diaz et al. (*4*, *5*).

W274 and R275 would be predicted on the basis of this structural alignment.

Although the structural alignment indicates that W274 of pol λ probably interacts with the DNA similarly to H34 of pol β, the correspondence between the side-chain positions of residues W274 and H34 is not as good as that between residues R275 and K35. The agreement is, however, better than the structural alignment of H34 between the solution and crystal structures of the pol β lyase domain (Figure 5a). Indeed, the significant difference between the position of H34 and its associated helix B in the solution and crystal structures led to the proposal that pol β might undergo a conformational change upon binding gapped DNA, repositioning helix B away from the hydrophobic core of the domain in order to position H34 for a base stacking interaction with the exposed base of the template DNA on the downstream side of the gap (*19*). We note, however, that this proposal is at odds with the observation that the orientation of H34 in the crystal structure of uncomplexed pol β [1BPD (*17*)] is very similar to that in the complex with gapped DNA [1BPX (*8*)] (compare panels a and b of Figure 5). Hence, a comparison of the two crystal structures does not provide good support for this hypothesis. Surprisingly, the side chain of H34 appears to have a high degree of order in the solution structure of the pol β domain (*19*; Figure 6b), although the amide resonance of H34 in the HSQC spectrum of the 8 kDa domain of pol β was broadened beyond detection (*19*). This observation suggests a significant degree of conformational heterogeneity. Figure 5b shows a superposition of three structures: the NMR-determined solution structures of the 8 kDa domains of pol β [1DK3 (*19*)] and pol λ and the crystal structure of this domain in pol β taken from the full structure of a pol β complex with gapped DNA [1BPX (*8*)].

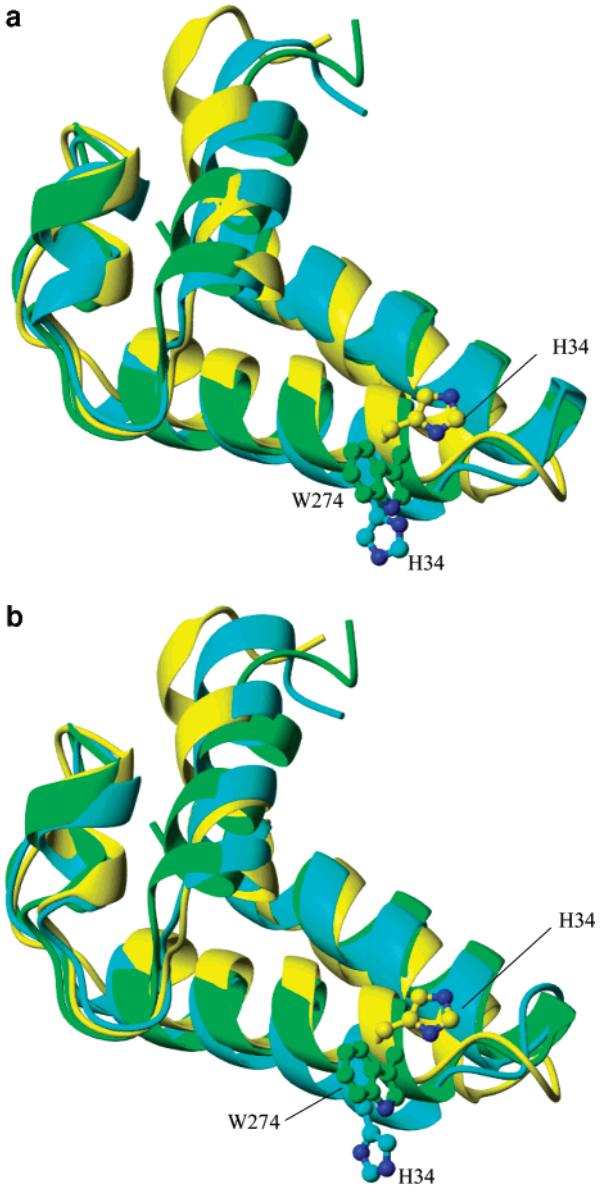

FIGURE 5: Ribbon diagrams comparing the positions of residues H34 (pol β) and W274 (pol λ) in various structures. The diagrams show a superposition corresponding to the solution structures of the 8 kDa domains of pol λ (residues 254−271 and 272−320) (green) with pol β (residues 13−30 and 32−80) (yellow) [1DK3 (*19*)]. Panel a also includes a superposition of the same region of pol β from the crystal structure of the uncomplexed polymerase [1BPD (*17*)], shown in cyan. Panel b also includes a superposition of the same residues of pol β from the crystal structure of pol β complexed with gapped DNA (cyan) [1BPX (*8*)]. The W274 side chain of pol λ is shown with the carbon atoms colored green. The H34 side chain of pol β is shown with the carbon atoms colored yellow in the solution structure and cyan in the crystal structure. The difference in position of the side chain in the solution structure illustrates how far helix B must move in order to be in the proper orientation for stacking with the exposed downstream template base of the gapped DNA substrate.

The difference in position of H34 between the two pol β structures illustrates how far this residue would need to move to adopt the position in the crystal structure. As shown in this figure, the side chain of W274 (pol λ) is positioned between the side chain of H34 in the solution and crystal structures of pol β. Nevertheless, this average structure arises from a superposition of a very broad range of conformations (Figure 6a). ARIA did not assign any long-range NOEs

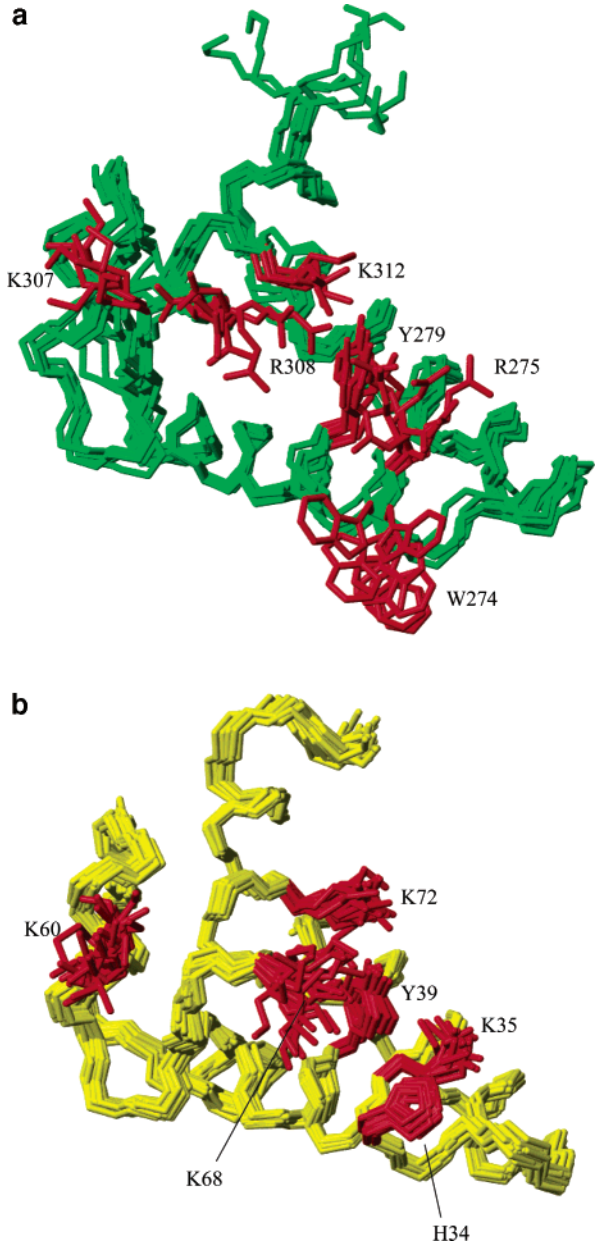

FIGURE 6: Comparison of the degree of ordering of selected residues in pol β and pol λ 8 kDa domains. (a) Mean backbone superposition (residues 254−320) of the seven lowest energy structures of the pol λ 8 kDa showing the side chains of potentially important catalytic and DNA binding residues. The backbone is colored green, and the side chains are colored red. The side chains of R275, Y279, and K312 are reasonably well ordered, while the side chains of W274 and R308 appear highly disordered due to the lack of long-range NOEs. (b) Mean backbone superposition (residues 14−80) of the 22 lowest energy structures of pol β 8 kDa domain of pol β [1DK2 (*19*)], showing the side chains of important catalytic and DNA binding residues. The backbone is colored yellow, and the side chains are colored red. The side chains of H34, K35, Y39, and K72, are well ordered, while the side chain of K68 appears highly disordered.

involving W274, and a manual check of the data verifies that no long-range NOEs involving W274 appear in either the ^{15}N- or ^{13}C-edited NOESY spectra. The lack of NOEs supports the conclusion that this residue is flexible in solution and thus available for the interaction with the DNA.

Basic Residues Involved in DNA Binding. The structures described here also provide insight into the basic residues involved in binding both gapped DNA and ssDNA. The

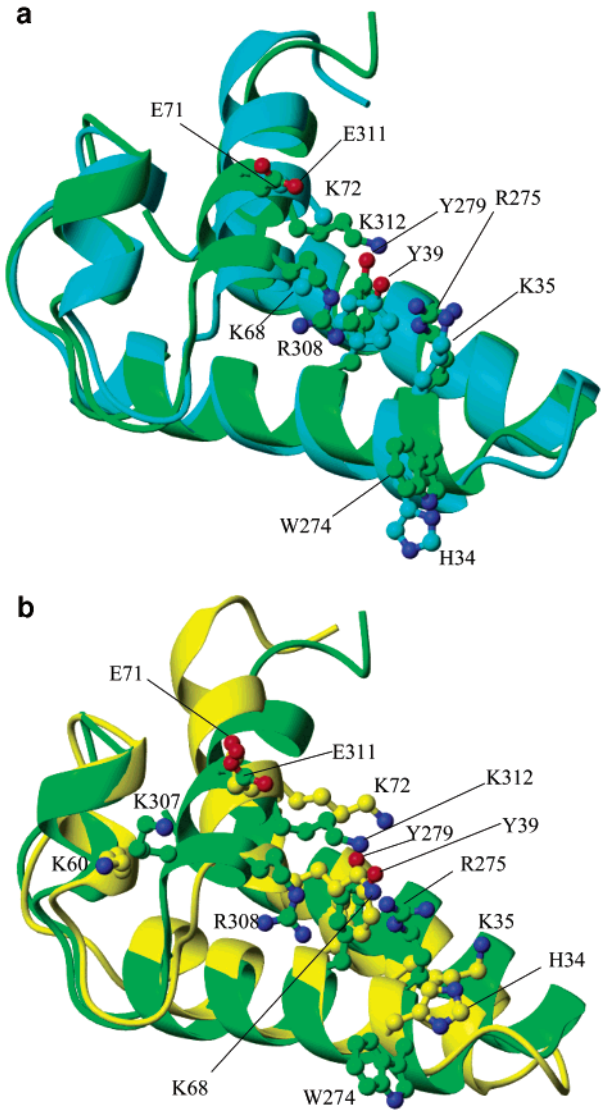

FIGURE 7: (a) Backbone overlay (residues 254−271 and 272−320) of the solution structure of the 8 kDa domains of pol λ (green) with the crystal structure (residues 13−30 and 32−80) of pol β (cyano) [1BPD (*17*)], showing the side chains of important catalytic and DNA binding residues in pol β and the corresponding residues in pol λ. The carbon atoms of the side-chain atoms are colored green in the pol λ structure and cyan in the pol β structure. (b) Backbone overlay (residues 254−271 and 272−320) of the solution structure of the 8 kDa domains of pol λ (green) with the solution structure of the 8 kDa domain (residues 13−30 and 32−80) of pol β (yellow) [1DK3 (*19*)], showing the side chains of important catalytic and DNA binding residues in pol β and the corresponding residues in pol λ. The carbon atoms of the side-chain atoms are colored green in the pol λ structure and yellow in the pol β structure. The side chain of residue K60 is shown in (b) but not (a) since structure 1BPD lacks data for this side chain.

positions of several basic residues proposed to be important for DNA binding and/or dRP lyase activity in pol β, H34, K35, K68, and K72, along with the corresponding residues of pol λ, W274, R275, R308, and K312, are shown in Figure 7. Figure 7a compares the 8 kDa domains for the solution structure of the pol λ and the crystal structure of pol β [1BPD (*17*)], while Figure 7b compares the solution structures of this domain in pol λ and pol β [1DK3 (*19*)]. The positions of the corresponding residues in the two domains are very similar. The side chains of K60 in pol β and K307 in pol λ are also shown in Figure 7b. Crystal structures of the complex

of pol β and gapped DNA place K35, K68, and K72 in close proximity to the 5′-phosphate in the gap (*8*, *47*). Mutagenesis data indicate that K35 is the key residue for 5′-phosphate recognition (*11*). In our structural alignment (Figure 7), the K35, K68, and K72 residues of pol β correspond to R274, R308, and K312 in pol λ, so that analogous electrostatic interactions with DNA would be predicted. In pol β K68 and K72 are contained in the HhH binding motif, which binds to the downstream oligo in gapped DNA (*8*). Mutagenesis results for pol β also have shown that K35, K60, and K68 are important for recognizing ssDNA (*11*). K60 is also contained in the HhH DNA binding motif. In contrast to the conservation of basic residues at positions 35, 68, and 72 of pol β, K60 in pol β is aligned with C298 in all of the proposed sequence alignments and in our structure. However, the lysine side chain of K307 in pol λ is positioned in close proximity to the K60 side chain of pol β. Hence, a K307−DNA interaction in pol λ is predicted to conserve the functionality of the K60−DNA interaction in pol β.

Residues Involved in dRP Lyase Reaction. A comparison of the structure of the pol λ 8 kDa domain presented here with that of the corresponding pol β domain provides a unique opportunity to consider the role of various residues in the dRP lyase reaction. K72 (pol β), proposed to be involved in Schiff base formation with the abasic deoxyribose, is conserved in all of the proposed sequence alignments, and its structural correspondence with K312 (pol λ) is similarly maintained in the structural alignment with pol β shown in Figure 7. In addition, the side chains of both residues are reasonably well ordered in both structures (Figure 6). These similarities imply that K72/K312 play similar roles in the two domains. Consistent with this prediction, Garcia-Diaz et al. (*4*) have trapped pol λ−DNA complexes using sodium borohydride, supporting the conclusion that the dRP lyase mechanism in pol λ also proceeds via a Schiff base intermediate. Studies of the K72A mutant of the pol β 8 kDa domain showed less than 10% of the dRP lyase activity of the native domain, while the triple alanine mutant K35A/K68A/K72A was devoid of activity (*11*). In our structural alignment, the K35 and K68 residues of pol β correspond to R274 and R308 in pol λ. Hence, neither residue can act as a nucleophile to form a Schiff base with the abasic deoxyribose. Alternatively, as noted above, residues R275 and R308 are well positioned to bind to the 5′-phosphate of the downstream primer. The structural alignment is thus completely consistent with the recent mass spectrometric data demonstrating a trapped Schiff base adduct with K72 of pol β (*52*).

Additional catalytic roles have also been postulated for these lysine residues in pol β. Feng et al. (*13*) have proposed that residue K35 or K68 in pol β could initiate the reaction by protonating the deoxyribose O-4′, leading to opening of the ring (see Figure 2 of ref *13*). As noted above, in pol λ arginine occupies both of the corresponding positions, and the guanidine side chain is a very poor proton donor. Interestingly, donation of a proton to O-4′ by K72 would result in the formation of the uncharged amine necessary for formation of the Schiff base, suggesting the possibility that both roles could be fulfilled by a single lysine residue. It also has been suggested that K35 may interact with the 3′-phosphate of the abasic site to stabilize the complex during the reaction (*19*, *48*), implying an analogous role for R275 in pol λ. Modeling studies have also placed the side chain of K68 in a position to donate a proton to the O-4′ during cleavage of the hemiacetal (*19*, *48*). However, the K68A mutant of pol β showed no effect on dRP lyase activity, and as noted above, pol λ contains an arginine residue at the corresponding position. The K68A mutant did, however, exhibit reduced ssDNA binding (*11*). Interestingly, the side chain of residue R308 in pol λ and K68 in pol β both appear disordered (Figure 6), implying that R308 in pol λ may also be important for ssDNA binding. The K60A mutant of pol β was also found to have reduced dRP lyase activity (*11*); however, the corresponding residue in pol λ, C298, cannot contribute to activity. On the other hand, as shown in Figure 7b and noted above, the side chain of K307 in pol λ is located in close proximity to the side chain of K60 in pol β, so K307 might function analogously with K60 in pol β.

In addition to the lysine residues, a number of other residues have been proposed to play a role in the dRP lyase reaction of the 8 kDa domain. Y39 in pol β has been proposed to assist in transferring a proton to the aldehyde of the abasic sugar preceding nucleophilic attack by K72. As shown in Figure 7, the orientation of Y279 in pol λ is in close agreement with that of Y39 in pol β. In addition, the side chains of both residues are reasonably well ordered in both structures (Figure 6). These similarities support the proposition that Y39/Y279 could play similar roles in the two domains. It has also been suggested that residue E71 or E26 could facilitate the reaction by removing the H-2′ proton after Schiff base formation [Feng et al. (*13*)]. The E71 residue is conserved in all proposed alignments, while E26 is not conserved. Thus, the structural comparison between pol λ and pol β suggests that E71 (E311 in pol λ) is the most likely residue to perform this function (Figure 7). Docking studies have suggested that the imidazole ring of H34 can act as a proton acceptor at the 1′-OH of the abasic site and stabilize the carbonium intermediate formed in the opening of the hemiacetal to produce the aldehyde form of the sugar (*48*). However, W274 could not play such a role. Further, the stacking interaction of H34, or in the case of pol λ, W274, with the template base would position these residues far from the C-1′ of the abasic residue on the downstream primer strand.

Electrostatic Surface of Pol λ. Panels a and b of Figure 8 illustrate the electrostatic surfaces of the pol λ and pol β 8 kDa domains, respectively. To a significant extent, the nature of the positively charged surface of the pol β lyase domain depends on assumptions about the protonation state of histidine. Assuming a positively charged imidazolium ion form of the side chain, the electrostatic surfaces appear to be generally similar (Figure 8). Alternatively, if the histidine is considered to be unprotonated, the extent of the contiguously positively charged region on the DNA binding surface is significantly greater for the pol λ lyase domain, which could result in tighter binding of the pol λ lyase domain relative to the pol β domain. The formation of a tighter DNA complex might influence the fidelity of the repair process, e.g., the extent of strand displacement (*5*).

CONCLUSIONS

In summary, the solution structure of the 8 kDa domain of pol λ has been determined by multidimensional NMR

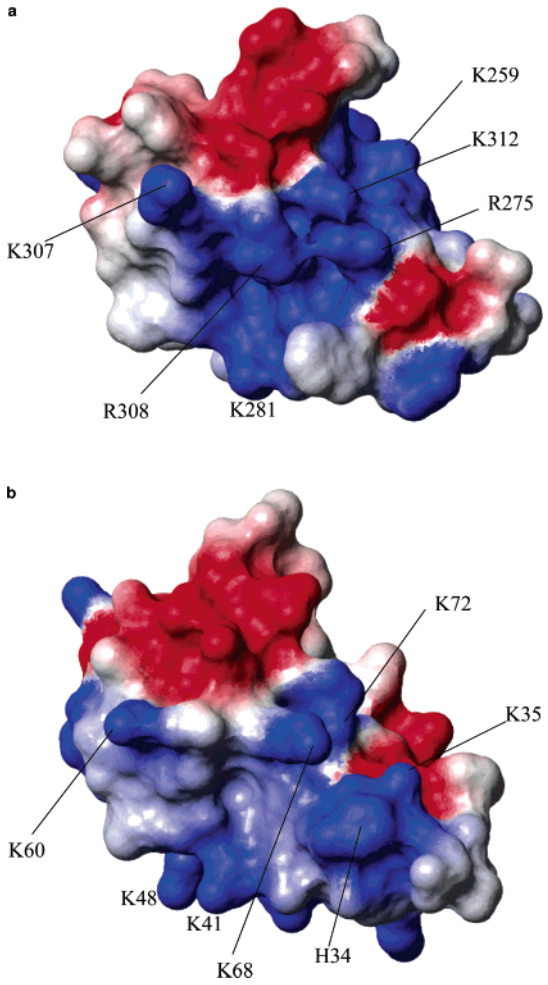

FIGURE 8: (a) Electrostatic surfaces of the solution structure of the pol λ and (b) pol β 8 kDa domains [1DK3 (*19*)], illustrating the greater extent of the positively charged DNA interaction surface on the surface of pol λ with respect to pol β.

methods. The structure is homologous with the previously determined solution and crystal structures of the 8 kDa domain of pol β in the intact enzyme. Both domains contain two pairs of antiparallel α-helices and a HhH DNA bindng motif (*18*, *19*) that is important for binding single-stranded DNA in pol β (*18*, *49*) and the downstream oligo in gapped DNA (*8*). The structural alignment has enabled a selection from among several previously proposed sequence alignments and allows identification of residues that play a role in the dRP lyase activity. Further, a structural comparison of the lyase domains has allowed a number of mechanistic proposals to be evaluated. In a few cases for which there is a nonconservative substitution in the sequence alignment, a structural comparison shows a positionally and, hence, probably a functionally equivalent residue, e.g., K60 in pol β and K307 in pol λ. Studies are currently underway to isolate a reduced form of the Schiff base intermediate suitable for NMR studies.

SUPPORTING INFORMATION AVAILABLE

Additional experimental details of the NMR experiments. This material is available free of charge via the Internet at http://pubs.acs.org.

REFERENCES

1. Aoufouchi, S., Flatter, E., Dahan, A., Faili, A., Bertocci, B., Storck, S., Delbos, F., Cocea, L., Gupta, N., Weill, J. C., and Reynaud, C. A. (2000) *Nucleic Acids Res. 28*, 3684−3693.
2. Garcia-Diaz, M., Dominguez, O., Lopez-Fernandez, L. A., de Lera, L. T., Saniger, M. L., Ruiz, J. F., Parraga, M., Garcia-Ortiz, M. J., Kirchhoff, T., del Mazo, J., Bernad, A., and Blanco, L. (2000) *J. Mol. Biol. 301*, 851−867.
3. Nagasawa, K., Kitamura, K., Yasui, A., Nimura, Y., Ikeda, K., Hirai, M., Matsukage, A., and Nakanishi, M. (2000) *J. Biol. Chem. 275*, 31233−31238.
4. Garcia-Diaz, M., Bebenek, K., Kunkel, T. A., and Blanco, L. (2001) *J. Biol. Chem. 276*, 34659−34663.
5. Garcia-Diaz, M., Bebenek, K., Sabariegos, R., Dominguez, O., Rodriguez, J., Kirchhoff, T., Garcia-Palomero, E., Picher, A. J., Juarez, R., Ruiz, J. F., Kunkel, T. A., and Blanco, L. (2002) *J. Biol. Chem. 277*, 13184−13191.
6. Kumar, A., Widen, S. G., Williams, K. R., Kedar, P., Karpel, R. L., and Wilson, S. H. (1990) *J. Biol. Chem. 265*, 2124−2131.
7. Prasad, R., Beard, W. A., and Wilson, S. H. (1994) *J. Biol. Chem. 269*, 18096−18101.
8. Sawaya, M. R., Prasad, R., Wilson, S. H., Kraut, J., and Pelletier, H. (1997) *Biochemistry 36*, 11205−11215.
9. Prasad, R., Beard, W., Strauss, P. P., and Wilson, S. H. (1998) *FASEB J. 12*, 241.
10. Prasad, R., Beard, W. A., Chyan, J. Y., Maciejewski, M. W., Mullen, G. P., and Wilson, S. H. (1998) *FASEB J. 12*, 244.
11. Prasad, R., Beard, W. A., Chyan, J. Y., Maciejewski, M. W., Mullen, G. P., and Wilson, S. H. (1998) *J. Biol. Chem. 273*, 11121−11126.
12. Prasad, R., Beard, W. A., Strauss, P. R., and Wilson, S. H. (1998) *J. Biol. Chem. 273*, 15263−15270.
13. Feng, J. A., Crasto, C. J., and Matsumoto, Y. (1998) *Biochemistry 37*, 9605−9611.
14. Srivastava, D. K., Vande Berg, B. J., Prasad, R., Molina, J. T., Beard, W. A., Tomkinson, A. E., and Wilson, S. H. (1998) *J. Biol. Chem. 273*, 21203−21209.
15. Sobol, R. W., Prasad, R., Evenski, A., Baker, A., Yang, X. P., Horton, J. K., and Wilson, S. H. (2000) *Nature 405*, 807−810.
16. Guex, N., and Peitsch, M. C. (1997) *Electrophoresis 18*, 2714−2723.
17. Sawaya, M. R., Pelletier, H., Kumar, A., Wilson, S. H., and Kraut, J. (1994) *Science 264*, 1930−1935.
18. Liu, D. J., Prasad, R., Wilson, S. H., DeRose, E. F., and Mullen, G. P. (1996) *Biochemistry 35*, 6188−6200.
19. Maciejewski, M. W., Liu, D. J., Prasad, R., Wilson, S. H., and Mullen, G. P. (2000) *J. Mol. Biol. 296*, 229−253.
20. Delaglio, F., Grzesiek, S., Vuister, G. W., Zhu, G., Pfeifer, J., and Bax, A. (1995) *J. Biomol. NMR 6*, 277−293.
21. Johnson, B. A., and Blevins, R. A. (1994) *J. Biomol. NMR 4*, 603−614.
22. Wittekind, M., and Mueller, L. (1993) *J. Magn. Reson., Ser. B 101*, 201−205.
23. Muhandiram, D. R., and Kay, L. E. (1994) *J. Magn. Reson., Ser. B 103*, 203−216.
24. Grzesiek, S., and Bax, A. (1992) *J. Am. Chem. Soc. 114*, 6291−6293.
25. Kay, L. E., Xu, G. Y., and Yamazaki, T. (1994) *J. Magn. Reson., Ser. A 109*, 129−133.
26. Ikura, M., Kay, L. E., and Bax, A. (1990) *Biochemistry 29*, 4659−4667.
27. Grzesiek, S., Anglister, J., and Bax, A. (1993) *J. Magn. Reson., Ser. B 101*, 114−119.
28. Logan, T. M., Olejniczak, E. T., Xu, R. X., and Fesik, S. W. (1992) *FEBS Lett. 314*, 413−418.
29. Logan, T. M., Olejniczak, E. T., Xu, R. X., and Fesik, S. W. (1993) *J. Biomol. NMR 3*, 225−231.
30. Montelione, G. T., Lyons, B. A., Emerson, S. D., and Tashiro, M. (1992) *J. Am. Chem. Soc. 114*, 10974−10975.
31. Gardner, K. H., Konrat, R., Rosen, M. K., and Kay, L. E. (1996) *J. Biomol. NMR 8*, 351−356.
32. Yamazaki, T., Formankay, J. D., and Kay, L. E. (1993) *J. Am. Chem. Soc. 115*, 11054−11055.
33. Kay, L. E., Ikura, M., Zhu, G., and Bax, A. (1991) *J. Magn. Reson. 91*, 422−428.
34. Vuister, G. W., and Bax, A. (1993) *J. Magn. Reson., Ser. B 102*, 228−231.

35. Pascal, S. M., Muhandiram, D. R., Yamazaki, T., Formankay, J. D., and Kay, L. E. (1994) *J. Magn. Reson., Ser. B 103*, 197−201.
36. Nilges, M. (1995) *J. Mol. Biol. 245*, 645−660.
37. Nilges, M. (1997) *Folding Des. 2*, S53−S57.
38. Nilges, M., and O'Donoghue, S. I. (1998) *Prog. Nucl. Magn. Reson. Spectrosc. 32*, 107−139.
39. Linge, J. P., and Nilges, M. (1999) *J. Biomol. NMR 13*, 51−59.
40. Brunger, A. T., Adams, P. D., Clore, G. M., DeLano, W. L., Gros, P., Grosse-Kunstleve, R. W., Jiang, J. S., Kuszewski, J., Nilges, M., Pannu, N. S., Read, R. J., Rice, L. M., Simonson, T., and Warren, G. L. (1998) *Acta Crystallogr., Sect. D: Biol. Crystallogr. 54*, 905−921.
41. Linge, J. P., O'Donoghue, S. I., and Nilges, M. (2001) *Nucl. Magn. Reson. Biol. Macromol. 339* (Part B), 71−90.
42. Nilges, M., Macias, M. J., Odonoghue, S. I., and Oschkinat, H. (1997) *J. Mol. Biol. 269*, 408−422.
43. Cornilescu, G., Delaglio, F., and Bax, A. (1999) *J.Biomol. NMR 13*, 289−302.
44. Koradi, R., Billeter, M., and Wuthrich, K. (1996) *J. Mol. Graphics 14*, 51.
45. Thayer, M. M., Ahern, H., Xing, D. X., Cunningham, R. P., and Tainer, J. A. (1995) *EMBO J. 14*, 4108−4120.
46. Mullen, G. P., and Wilson, S. H. (1997) *Biochemistry 36*, 4713−4717.
47. Pelletier, H., Sawaya, M. R., Wolfle, W., Wilson, S. H., and Kraut, J. (1996) *Biochemistry 35*, 12742−12761.
48. Mullen, G. P., Antuch, W., Maciejewski, M. W., Prasad, R., and Wilson, S. H. (1997) *Tetrahedron 53*, 12057−12066.
49. Liu, D. J., DeRose, E. F., Prasad, R., Wilson, S. H., and Mullen, G. P. (1994) *Biochemistry 33*, 9537−9545.
50. Laskowski, R. A., Macarthur, M. W., Moss, D. S., and Thornton, J. M. (1993) *J. Appl. Crystallogr. 26*, 283−291.
51. Rullmann, J. A. C. (1996), AQUA, Computer program, Department of NMR Spectroscopy, Bijvoet Center for Biomolecular Research, Utrecht University, The Netherlands.
52. Deterding, L. J., Prasad, R., Mullen, G. P., Wilson, S. H., and Tomer, K. B. (2000) *J. Biol. Chem. 275*, 10463−10471.

BI034298S